Nuclear Science and Techniques (2025) 36:66
https://doi.org/10.1007/s41365-025-01662-y

Measurements of ^{27}Al(γ, n) reaction using quasi-monoenergetic γ beams from 13.2 to 21.7 MeV at SLEGS

Pu Jiao[1,2] · Zi-Rui Hao[2] · Qian-Kun Sun[3,4] · Long-Xiang Liu[2] · Hang-Hua Xu[2] · Yue Zhang[2] · Meng-Die Zhou[2,5] · Zhi-Cai Li[2,6] · Wen Luo[6] · Yu-Xuan Yang[3,7] · Sheng Jin[3,4] · Kai-Jie Chen[3,8] · Shan Ye[2,9] · Zhen-Wei Wang[3,4] · Yu-Ting Wang[1] · Hui-Ling Wei[1] · Yao Fu[3] · Kun Yu[10,11] · Hong-Wei Wang[2,3,4] · Gong-Tao Fan[2,3,4] · Chun-Wang Ma[1,12]

Received: 4 October 2024 / Revised: 17 December 2024 / Accepted: 20 December 2024 / Published online: 25 February 2025

Abstract

The accurate photoneutron cross section of the ^{27}Al nucleus has a significant impact on resolving differences in existing experimental data and enhancing the precision of nuclear reaction rate calculations for ^{26}Al in nuclear astrophysics. The photoneutron cross sections for the ^{27}Al(γ, n)^{26}Al reaction, within the neutron separation energy range of 13.2–21.7 MeV, were meticulously measured using a new flat efficiency detector array at the Shanghai Laser-Electron Gamma Source. The uncertainty of the data was controlled to below 4% throughout the process, and inconsistencies between the present data and existing data from different gamma sources, as well as the TENDL-2021 data, are discussed in detail. These discussions provide a valuable reference for addressing discrepancies in the ^{27}Al(γ, n)^{26}Al cross-section data and improving related theoretical calculations.

Keywords Photoneutron cross section · Flat efficiency detector · Laser Compton scattering · γ Rays · SLEGS

1 Introduction

The investigation of the giant dipole resonance (GDR) [1] in nuclear physics, particularly from the 1960 s to the 1980 s, involved extensive measurements of photoneutron cross sections. Comprehensive documentation of GDR data is now available on various web platforms [2]. Specifically,

Pu Jiao and Zi-Rui Hao have contributed equally to this work.

This work was supported by the National key R&D program (Nos. 2023YFA1606901 and 2022YFA1602404), the National Natural Science Foundation of China (Nos. 12375123 and 12388102), and the Natural Science Foundation of Henan Province (No. 242300422048).

✉ Gong-Tao Fan
fangt@sari.ac.cn

✉ Chun-Wang Ma
machunwang@126.com

1 School of Physics, Centre for Theoretical Physics, Henan Normal University, Xinxiang 453007, China

2 Shanghai Advanced Research Institute, Chinese Academy of Sciences, Shanghai 201204, China

3 Shanghai Institute of Applied Physics, Chinese Academy of Sciences, Shanghai 201800, China

4 University of Chinese Academy of Science, Beijing 100080, China

5 College of Physics, Centre for Theoretical Physics, Henan Normal University, Xinxiang 453007, China

6 School of Nuclear Science and Technology, University of South China, Hengyang 421001, China

7 School of Physics, Zhengzhou University, Zhengzhou 450001, China

8 ShanghaiTech University, Shanghai 201210, China

9 China Institute of Atomic Energy, Beijing 102413, China

10 School of Physics, Henan Normal University, Xinxiang 453007, China

11 Henan Key Laboratory of Infrared Material & Spectrum Measures and Applications, Henan Normal University, Xinxiang 453007, China

12 Institute of Nuclear Science and Technology, Henan Academy of Sciences, Zhengzhou 450046, China

research on GDR photoreactions was facilitated by the use of quasi-monochromatic γ rays generated through positron annihilation in flight (PAIF) at two prominent research institutions: Saclay (France) and Lawrence Livermore National Laboratory (USA) [3]. Since 2000, research on low-energy photonuclear reactions has been revitalized, driven not only by advancements in studies of low-energy electric dipole strength (e.g., pygmy dipole resonance, PDR) [4], but also by investigations into the origins of elemental nucleosynthesis in nuclear astrophysics [5, 6]. The development of a new γ-ray source based on laser Compton scattering (LCS) has introduced an innovative approach for the systematic study of γ induced nuclear reactions with monoenergetic incident energy [7]. This resurgence has been further supported by the application of LCS technology at leading institutions and facilities, including the National Institute of Advanced Industrial Science and Technology (AIST) [8–10], NewSUBARU BL01 [11–13], and HIγS [14, 15].

The ^{27}Al(γ, n)^{26}Al reaction plays a crucial role in astrophysical processes, particularly in high-temperature and high-density environments such as star cores, supernova explosions, and other high-energy events [16]. This reaction, initiated by the absorption of high-energy γ-rays by the ^{27}Al nucleus, serves as a bridge between nuclear physics and astrophysics. By employing these γ-rays, the reaction facilitates the production and transformation of nuclei, offering valuable insights into the evolution of the universe, the complexities of nuclear reaction networks, and the mechanisms of energy transfer in astrophysical environments. However, significant discrepancies in the measured ^{27}Al(γ, n)^{26}Al reaction data have been observed, largely due to variations in measurement techniques or data analysis methods. These inconsistencies complicate efforts to accurately understand the underlying physical mechanisms.

Traditional methods for measuring the cross sections of ^{27}Al(γ, n)^{26}Al, such as bremsstrahlung [17, 18] unfolding techniques or in-flight annihilation of monochromatic positrons, often yield conflicting results, with discrepancies ranging from 20 to 50% [19]. The bremsstrahlung method is prone to systematic errors due to mathematical unfolding processes, while the in-flight annihilation method suffers from intensity calibration issues of the photon beam, resulting in systematic errors of approximately 7%, even at the peak values of the GDR. In contrast, the use of LCS γ rays for ^{27}Al(γ, n)^{26}Al measurements offers significant advantages, primarily because they are free from low-energy tail effects. In this study, the energy dependence of the ^{27}Al(γ, n)^{26}Al cross sections was systematically measured using the LCS γ-ray method. While the derivation of monoenergetic cross sections using an LCS source is more complex and requires longer experimental time compared to bremsstrahlung sources, the methods and data reduction techniques employed in this study were improved. The results were then compared with previous measurements, highlighting significant discrepancies and uncertainties associated with each method.

2 Experiment

A schematic illustration of the SLEGS [20] and the corresponding experimental setup are presented in Fig. 1. After traversal through the collimation system, the LCS γ-ray beams strike metallic ^{27}Al targets located at the central focus of the Flat Efficiency Detector (FED).

2.1 Brief introduction to SLEGS beamline

The SLEGS beamline [20–26] at the Shanghai Synchrotron Radiation Facility (SSRF) delivers quasi-monochromatic γ rays with maximum scattering energies (E_γ) ranging from 0.66 to 21.7 MeV. This beamline employs inverse Compton scattering technology, wherein photons from a 10,640 nm, 100 W CO_2 laser collide with 3.5 GeV electrons circulating in the SSRF storage ring. The energy of the γ-ray beam is tuned in the slant-scattering mode with a minimum step size of 10 keV, enabling precise mapping of cross sections. This precision surpasses that of γ-ray beams generated under backward scattering at the AIST [7] and NewSUBARU BL01 beamlines [27].

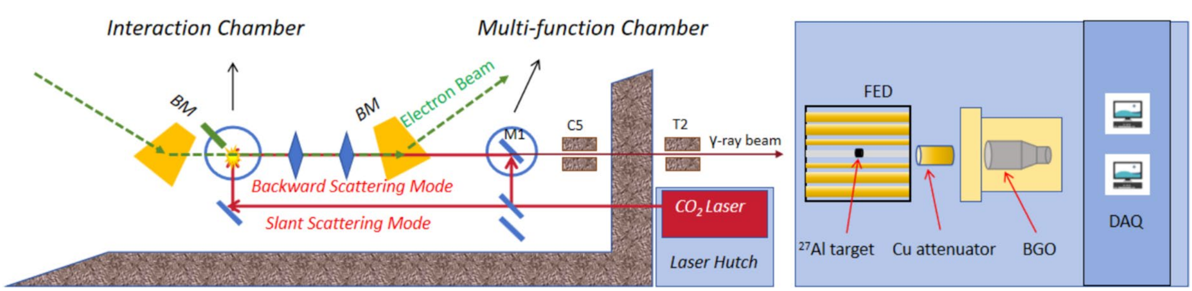

Fig. 1 (Color online) The setup of SLEGS. A set of two collimators of 5 mm (C5) and 2 mm (T2) aperture was used for the ^{27}Al(γ, n)^{26}Al in experiment

The experiment was conducted using the SSRF storage ring, which operated in top-up mode with a beam current of 160–210 mA and an energy of 3.5 GeV. A CO_2 laser, delivering an average power of 5–20 W at a frequency of 1 kHz and a pulse width of 50 μd, was used to generate γ-rays. These γ-rays were collimated with a C5T2 double collimator. By varying the interaction angle from 102° to 180°, γ-rays with theoretical energies ranging from 13.16 to 21.73 MeV were produced. Within this energy range, 38 energy points of the ^{27}Al(γ, n)^{26}Al reaction cross sections were measured. The incident γ-ray spectrum on the detector was derived using the direct unfolding method described in [28–30]. Figure 2 presents the detector response spectrum (blue dashed-dotted line) and the unfolded spectra at slant-scattering angles of 103°, 124°, and 155° (red dashed lines). The reconstructed spectrum, obtained by convolving the incident γ-ray spectrum with the simulated detector response matrix [31], is shown as a black line and aligns well with the measured spectrum. The theoretical Compton-edge energies for interactions at 103°, 124°, and 155° were calculated to be 13.37, 16.96, and 20.73 MeV, respectively. These values closely match the energies at the half-peak height on the high-energy side of the incident γ-ray spectrum, confirming the accuracy of the measurements.

2.2 Al Target

The aluminum (Al) target consisted of five 10 mm in diameter and 25 mm in thickness of ^{27}Al isotopes with 100% abundance and 99.99% purity. The detailed specifications can be found in Table 1.

The targets were positioned in a polythene sample holder with a 10-mm diameter window. Given that the LCS γ-ray beams had a diameter of approximately 4 mm at the target position, the 10 mm diameter window was sufficient to allow accurate measurement of the target without interference from neutrons originating in the polythene.

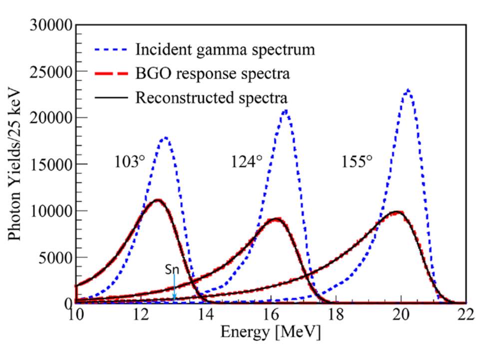

Fig. 2 (Color online) A typical γ spectrum obtained by BGO detector (red dash line) and the corresponding unfolded γ spectrum (blue dash-dot line). The reconstructed spectrum is shown as black line. The spectrum is measured with C5T2

Table 1 Elemental components (in ppm) of the ^{27}Al target used in experiments

Mn	Mg	Si	Ti	V	Cr
0.13	1.35	2.87	0.26	0.24	0.20
Fe	Ni	Cu	Zn	Ga	
3.06	0.08	3.19	0.26	0.34	
Total chemical impurities ^{27}Al > 99.99 %					
Physical form					
Weight (g)	Diameter (mm)	Total thickness (mm)	Density (g/cm^3)		
5.21	10.00	24.74	2.68		

2.3 Measurements

The details of the measurements and analyses are provided in Ref. [32], and are only briefly summarized here. To determine the cross sections, the measured quantities included the energy distribution and flux of LCS γ-rays irradiating the sample, as well as the number of neutrons generated from (γ, n) reactions. The energy distribution of the LCS γ-rays was measured using a BGO detector and deduced by unfolding the charge integration spectrum with the BGO response functions.

In the FED system, proportional counters are embedded in moderators such as paraffin or polyethylene to thermalize the emitted neutrons from the reaction. The large neutron capture cross section of ^{3}He for thermal neutrons makes it an ideal medium for neutron detection. A flat efficiency response is achieved by optimizing the placement of the ^{3}He counters within the moderator. Typically, ^{3}He counters are arranged in concentric rings, with the efficiency of the inner ring being the highest but decreasing rapidly as neutron energy increases. The outer rings compensate for this efficiency loss at higher neutron energies, resulting in a nearly uniform total detector efficiency across a broad energy range. At NewSUBARU [33], the ^{3}He FED, composed of ^{3}He proportional counters, was demonstrated to be an effective tool for studying photoneutron cross sections.

A new ^{3}He Flat Efficiency Detector (FED) was developed at the SLEGS station [32]. Figure 3 illustrates the FED system structure, featuring 26 ^{3}He proportional counters integrated into a polyethylene moderator. These counters were arranged in three concentric rings at distances of 65 mm, 110 mm, and 175 mm from the central beam axis. The moderator included a central tunnel to allow the gamma beam to pass through, with the target positioned at the center of the three rings. The ^{3}He proportional counters had cylindrical sensitive volumes, each 500 mm in length, pressurized with 2 atm of ^{3}He gas. The counters in Ring-1 (inner ring) had a diameter of 1 inch, while those in Ring-2 (middle ring) and Ring-3 (outer ring)

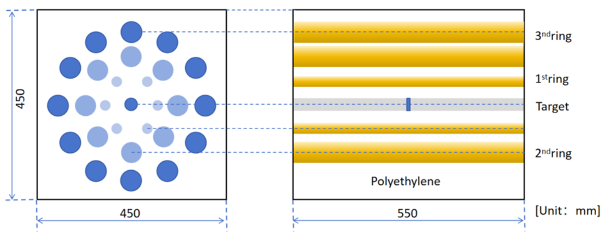

Fig. 3 (Color online) Structure of the FED. The left and right panels denote the front view and the lateral profile of FED

had a diameter of 2 inches. The counters were constructed with thin stainless steel walls, ensuring low background noise, high γ resistance, and good pressure tolerance. The inner polyethylene moderator measured 450 mm $\times$ 450 mm $\times$ 550 mm along the beam direction. To minimize interference from environmental neutrons, 2 mm-thick cadmium (Cd) sheets were used to cover all six surfaces of the moderator. The entire assembly, including the inner moderator and Cd sheets, was sealed with polyethylene plates for added stability and neutron shielding. The ^{3}He proportional counters were powered by a CAEN SY4527LC crate, maintaining a high-voltage deviation of no more than 1 V. Initial signals from the ^{3}He counters were routed to preamplifiers and subsequently processed using a Mesytec MDPP-16 digital pulse processor. Renowned for its high time and amplitude resolution, this processor produced precise reconstructed waveforms. Data acquisition was handled by the MVME DAQ system. Figure 4 shows the simulated efficiency curve based on the Geant4 model of the detector. The total detector efficiency increased from 35.6% at 50 keV to 42.3% at 1.65 MeV, followed by a gradual decrease to 40.7% at 3 MeV for the average neutron energy. Efficiency

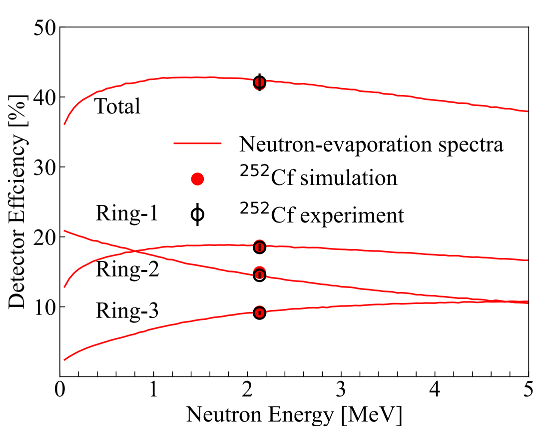

Fig. 4 (Color online) The total detector efficiency and the efficiencies of individual rings. The detector efficiency curves were simulated by neutron-evaporation spectra and monochromatic neutrons. The red dots are given by the neutron spectrum described by the Maxwell–Boltzmann distribution, at the average neutron energy (T = 1.42 MeV) of ^{252}Cf [34]

calibration with a ^{252}Cf source yielded a value of 42.1 $\pm$ 1.3% at 2.13 MeV, the average energy of neutrons emitted by ^{252}Cf, as indicated on the curve. The uncertainty of the efficiency curve was evaluated by varying parameters such as the moderator density, gas pressure, and counter-sensitive volumes. While the efficiency curve provides an estimate for a range of neutron spectra, precise characterization of neutron detector efficiency for specific energy profiles requires calculation of the weighted average efficiency.

The ring-ratio technique, which exploits the energy dependence of the Ring Ratio, was originally developed by Berman et al. [5, 33, 35]. Figure 5 presents the Geant4 simulations illustrating the Ring Ratios as functions of the neutron energy.

3 Analysis and Discussion

3.1 Monochromatic Approximation

The cross section in the monochromatic approximation is given by

$$\int_{S_n}^{E_{\max}} n_\gamma(E)\sigma(E)\mathrm{d}E = \frac{N_\mathrm{n}}{N_\gamma N_\mathrm{t}\xi\epsilon_\mathrm{n}}. \tag{1}$$

By contrast, for $n_\gamma(E)$, the energy distribution of the LCS γ -ray beams was normalized to unity in the energy region of integration. $\sigma(E)$ represents the photoneutron cross section and N_n is the number of detected neutrons. N_t denotes the number of target nuclei per unit area and N_γ represents the number of γ particles incident on the target with energies above the neutron threshold. The correction factor for a thick target measurement is expressed as $\xi = (1 - e^{\mu t})/\mu t$, where μ denotes the linear attenuation coefficient of photons in the target material and t represents the thickness of the target. The symbol ϵ_n represents the neutron detection efficiency.

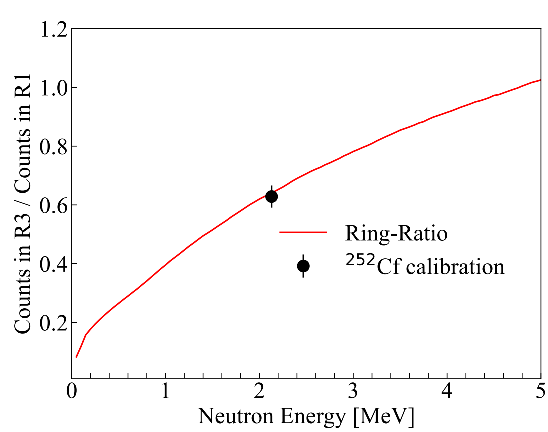

Fig. 5 (Color online) The ring-ratio curve of the FED array

$$\sigma^{E_{\max}}_{(\gamma,n)} = \frac{N_{\rm n}}{N_\gamma N_{\rm t}\xi\epsilon_{\rm n}}. \tag{2}$$

Assuming $E_{\max}$ represents the energy of the LCS γ-ray beams, the photoneutron cross sections are obtained at the energy in the monochromatic approximation using Eq. (2). The γ beam was collimated to a diameter of 2 mm using a three-hole collimator. However, because of the energy dispersion of the LCS γ-ray beams (see Fig. 2); the monochromatic approximation is inadequate for determining photoneutron cross sections.

In the experiment, the laser pulse period was 1000 µs, consisting of a 50 µs laser on time and a 950 µs off time. This pulse period facilitates inverse Compton scattering between the laser and electron beam, resulting in the production of γ-rays with inherent time broadening. Consequently, the neutrons generated by interaction with the experimental target exhibited time broadening. To accurately count the number of neutrons, an FED array is employed, which involves identifying the flat efficiency zone and measuring the neutron counts within this region. However, the flat efficiency zone varies with the neutron energy as well as other factors such as the size of each ring and ambient conditions such as the counter gas pressure. Therefore, it is necessary to determine the flat efficiency region for each ring at different energy levels, and use the median method to establish the optimal efficiency point. This strategy ensures a more reasonable statistical analysis of the neutron counts.

3.2 Unfolding Photoneutron Cross Sections

Approximating the integral in Eq. (1) with a summation of each γ-beam profile, the unfolding problem can be expressed as a set of linear equations. The unknown cross section σ can be determined by solving the equations for the system $\sigma_{\rm f} = \mathbf{D}\sigma$, where $\sigma_{\rm f}$ represents the folded cross section with beam profile $\mathbf{D}$. This approach solves the unfolding problem by formulating it as a linear algebraic problem.

$$\begin{pmatrix}\sigma_1\\ \sigma_2\\ \vdots\\ \sigma_N\end{pmatrix}_{\rm f} = \begin{pmatrix} D_{11} & D_{12} & \cdots & D_{1M}\\ D_{21} & D_{22} & \cdots & D_{2M}\\ \vdots & \vdots & \ddots & \vdots\\ D_{N1} & D_{N2} & \cdots & D_{NM}\end{pmatrix}\begin{pmatrix}\sigma_1\\ \sigma_2\\ \vdots\\ \vdots\\ \sigma_M\end{pmatrix}. \tag{3}$$

Matrix $\mathbf{D}$ is composed of the normalized incident gamma energy distributions from $S_{\rm n}$ to $E_{\max}$ at the discrete beam energies (E_γ). The system of linear equations presented in Eq. (3) is underdetermined, making it impossible to directly extract the true vector σ by matrix inversion. To determine σ, the following folding iteration method was employed [36, 37]:

The process starts at the zeroth iteration of a constant trial function σ_0. This initial vector is multiplied with $\mathbf{D}$, and the zeroth folded vector is obtained $\sigma^0_{\rm f} = \mathbf{D}\sigma^0$. The next trial input function is denoted as σ_1. This is realized by adding the difference between the experimentally measured $\sigma_{\rm exp}$ and folded spectrums $\sigma^0_{\rm f}$ to $\mathbf{D}\sigma^0$. To enable the addition of folded and input vectors, spline interpolation is initially performed on the folded vector to ensure that both vectors have matching dimensions. The new input vector is

$$\sigma^1 = \sigma^0 + (\sigma_{\rm exp} - \sigma^0_{\rm f}). \tag{4}$$

The above steps are iterated i times, yielding

$$\sigma^i_{\rm f} = \mathbf{D}\sigma^i, \tag{5}$$

and

$$\sigma^{i+1} = \sigma^i + (\sigma_{\rm exp} - \sigma^i_{\rm f}). \tag{6}$$

The updated input vector is determined iteratively until convergence is achieved. The convergence criterion is satisfied when $\sigma^{i+1}_{\rm f}$ approximates $\sigma_{\rm exp}$ within statistical error limits. Convergence was quantitatively assessed by computing the reduced χ^2 between $\sigma^{i+1}_{\rm f}$ and $\sigma_{\rm exp}$ at the end of each iteration. Typically, approximately three iterations are adequate to achieve convergence, which is characterized by a reduced χ^2 value approaching one.

The monochromatic cross sections of the ^{27}Al(γ, n)^{26}Al reaction were derived using the unfolding iteration method. Figure 6 compares the quasi-monochromatic and monochromatic cross sections for ^{27}Al. Statistical uncertainties are attributed solely to neutron counts, as a high number of γ-ray counts results in negligible uncertainties. The total uncertainty encompasses statistical, systematic, and methodological components. The total uncertainty estimate for

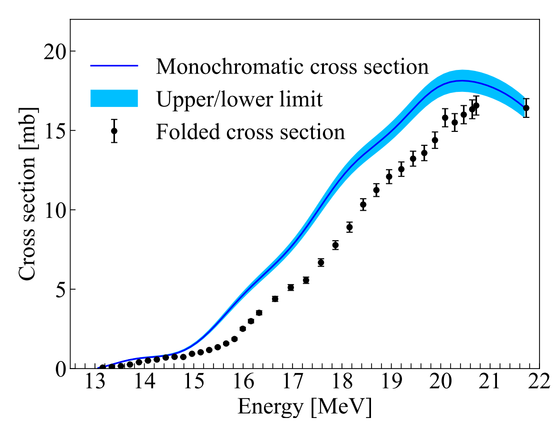

Fig. 6 (Color online) Cross sections of ^{27}Al(γ, n)^{26}Al measured at SLEGS. The dots are the folded cross section and the line with shaded area is the unfolded (monochromatic) cross section

^{27}Al(γ, n)^{26}Al is less than 4%, except for the data points corresponding to lower cross-sectional values and energies of 21.7 MeV. The cross sections for the SLEGS experiment were comparable to or even higher than some of the datasets in the EXFOR database. The conclusions regarding systematic uncertainties are as follows:

- The total uncertainty in the efficiency of the neutron detector is 3.0%.
- The uncertainty in the reconstructed incident energy spectrum due to the external copper attenuator and the target is 0.50%.
- The uncertainty in the target thickness is estimated to be less than 0.10%.

The uncertainties associated with data processing for the cross-sectional calculations are summarized below.

- The neutron count extraction algorithm introduces an uncertainty of approximately 2%.
- The BGO detectors exhibit 100% efficiency; when combined with the modeled BGO reaction matrix, the overall uncertainty is approximately 1%.

First, the measured cross sections for the ^{27}Al(γ, n)^{26}Al reaction were compared with TENDL-2021 [38] and available experiments from various γ ray sources. In Fig. 7, data from Baglin [39] and Mutsuro [40], originate from gamma sources induced by bremsstrahlung γ beams, while the data from Fultz [41] and Veyssiere [42] are derived from gamma sources associated with PAIF. It can be visually discerned that there are distinct segmented characteristics in the differences between the datasets.

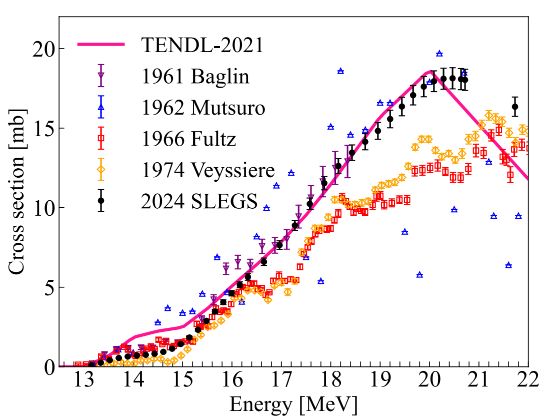

Fig. 7 (Color online) The measured cross section for ^{27}Al(γ, n)^{26}Al (solid circles) at SLEGS and comparison with existing data. The solid line denotes the TENDL-2021 evaluation. Results measured with bremsstrahlung γ rays (Baglin 1961 and Mutsuro 1962) are shown by filled inverted triangles and filled triangles, respectively. Results measured with PAIF γ rays (Fultz 1966 and Veyssiere 1974) are indicated by squares and diamonds, respectively

The uncertainty of the specific data is shown, as the measured data in the energy region below 16.3 MeV are in good agreement with the data obtained by Fultz using a PAIF gamma source. In the energy region above 16.3 MeV, the measured data are significantly higher than the data obtained by Fultz and Veyssiere using PAIF γ sources but agree with the data obtained by Baglin et al. using bremsstrahlung γ sources. With respect to the global structure of the data, this dataset shows high consistency with the TENDL-2021 [38] data and exhibits more uniform smoothness, whereas the Fultz and Veyssiere datasets display multiple oscillations during the increased cross section. These oscillations show worse agreement with the calculations from relevant nuclear reaction models, such as the quasiparticle random phase approximation (QRPA) [43], and are particularly pronounced during the ascent of the QRPA ^{27}Al(γ, n)^{26}Al cross section. The implications of this work are significant for both the evaluation of nuclear data and the optimization of the parameters of the theoretical model.

As discussed in Ref. [44], the ratios of the integral cross sections provide a clear indication of the systematic differences among the various data compilations. The integral cross sections in the S_n and S_{max} regions are as follows:

$$\sigma^{\text{int}} = \int_{S_n}^{S_{\max}} \sigma(E)\mathrm{d}E. \tag{7}$$

Experiments on the reactions ^{197}Au(γ, n) and ^{159}Tb(γ, n) were performed using SLEGS [32]. Comparison of ^{197}Au(γ, n) reaction data with the findings of Itoh et al [33] revealed an integrated cross-sectional difference of approximately 0.4%, which underscores the reliability of SLEGS in both measurement procedures and data analysis. Based on these reliable experimental data, the integral ratios of the photoneutron cross sections were calculated for energy ranges from S_n to 16.3 MeV, 16.3 MeV to E_{max} and S_n to E_{max}, as shown in Table 2. In the energy range from S_n to 16.3 MeV, the experimental results in this study differ from the Fultz data by only 4%, whereas the discrepancy with other datasets exceeds 30%. In the energy range of 16.3 MeV to E_{max}, the

Table 2 Integral cross-section ratio

Ratio relation	σ^{int} ratio		
	S_n–16.3 MeV	16.3 MeV–E_{max}	S_n–E_{max}
$\sigma^{\text{int}}_{\text{TENDL}}/\sigma^{\text{int}}_{\text{SLEGS}}$	1.46	0.96	0.99
$\sigma^{\text{int}}_{\text{Baglin}}/\sigma^{\text{int}}_{\text{SLEGS}}$	1.36	1.03	1.11
$\sigma^{\text{int}}_{\text{Mutsuro}}/\sigma^{\text{int}}_{\text{SLEGS}}$	1.63	0.92	0.97
$\sigma^{\text{int}}_{\text{Fultz}}/\sigma^{\text{int}}_{\text{SLEGS}}$	1.04	0.72	0.74
$\sigma^{\text{int}}_{\text{Veyssiere}}/\sigma^{\text{int}}_{\text{SLEGS}}$	0.69	0.77	0.75

results from this work show a difference of 3% compared to Baglin's results and 4% compared to TENDL, with discrepancies from other datasets ranging between 8% and 28%. In general, the TENDL evaluated data agree with the measured data in this work across the energy range of 13–20 MeV. However, the rapid decrease in cross-section values after 20 MeV observed in the TENDL data is not physically reasonable. The differences between the data from this measurement and those from other laboratories range from 3% to 25%. Notably, after the energy exceeded 20 MeV, the relatively large energy intervals between the TENDL data points and the unusually rapid decline in the high-energy segment make the discrepancies between TENDL and the data from other laboratories more pronounced. The cross-section rise observed in this work was smooth, with no resonance structure peaks detected. This suggests that the resonance structures measured in other laboratories may be artifacts arising from the process of solving single-energy cross sections. Considering the variations in the data structure between the measured results, the data presented here have significant implications for refining nuclear data evaluations, optimizing theoretical model parameters, resolving discrepancies in the $^{27}Al(\gamma, n)^{26}Al$ reaction cross section, and improving the understanding of its underlying nuclear structure.

4 Summary

Measurements of cross sections for the $^{27}Al(\gamma, n)^{26}Al$ reactions were conducted across an incident energy range of 13.2 to 21.7 MeV using the ^{3}He FED system developed at SLEGS. The precision of these measurements was underscored by an overall uncertainty margin maintained below 4%. Through detailed deviation and ratio analyses, a comprehensive comparison was made between the current photoneutron cross-sectional data and previous datasets, helping to resolve longstanding discrepancies within the ^{27}Al photonuclear cross-sectional data. These efforts also contributed to the refinement of theoretical nuclear reaction models. Given the critical importance of the ^{27}Al photoneutron cross section in aerospace and astrophysics applications, plans are underway to extend the energy range of future investigations. This expansion will aim to provide a more thorough examination of both the $^{27}Al(\gamma, n)^{26}Al$ and $^{27}Al(\gamma, 2n)^{25}Al$ cross sections.

Acknowledgements The authors thank the SSRF team for stable maintenance of the electron beam during the experiments. The authors also thank Professors Yifei Niu (Lanzhou U.), Danyang Pang (Beihang U.), and Chuangye He (CIAE, China) for useful discussions.

Author Contributions All authors contributed to the study conception and design. Material preparation, data collection, and analysis were performed by Z-RH, Q-KS, L-XL, H-HX, YZ, M-DZ, Z-CL, WL, Y-XY, SJ, K-JC, SY, Z-WW, Y-TW, H-LW, YF, KY, H-WW, G-TF and C-WM. The first draft of the manuscript was written by PJ, and all authors commented on previous versions of the manuscript. All authors read and approved the final manuscript.

Data Availability The data that support the findings of this study are openly available in Science Data Bank at https://cstr.cn/31253.11.sciencedb.j00186.00535 and https://www.doi.org/10.57760/sciencedb.j00186.00535.

Declarations

Conflict of interest Chun-Wang Ma and Hong-Wei Wang are the editorial board members for Nuclear Science and Techniques and were not involved in the editorial review, or the decision to publish this article. All authors declare that there is no conflict of interest.

References

1. S.S. Dietrich, B.L. Berman, Atlas of photoneutron cross sections obtained with monoenergetic photons. Tech. Rep., Univ. of California, Livermore, **38**, 199 (1988). https://doi.org/10.1016/0092-640X(88)90033-2
2. M. Chadwick, P. Oblozinsky, A. Blokhin et al., Handbook on Photonuclear Data for Applications: Cross Sections and Spectra, IAEA Tech-Doc 1178 (2000)
3. P. Mohr, K. Vogt, M. Babilon et al., Experimental simulation of a stellar photon bath by bremsstrahlung: the astrophysical γ -process. Phys. Lett. B **488**, 127 (2000). https://doi.org/10.1016/S0370-2693(00)00862-5
4. D. Savran, T. Aumann, A. Zilges, Experimental studies of the pygmy dipole resonance. Prog. Part. Nucl. Phys. **70**, 210 (2013). https://doi.org/10.1016/j.ppnp.2013.02.003
5. B.L. Berman, S. Fultz, Measurements of the giant dipole resonance with monoenergetic photons. Rev. Mod. Phys. **47**, 713 (1975). https://doi.org/10.1103/RevModPhys.47.713
6. H.K. Wu, X.Y. Wang, Y.M. Wang et al., Fudan multi-purpose active target time projection chamber (fMeta-TPC) for photonuclear reaction experiments. Nucl. Sci. Tech. **35**, 200 (2024). https://doi.org/10.1007/s41365-024-01576-1
7. H. Ohgaki, S. Sugiyama, T. Yamazaki et al., Measurement of laser-induced Compton backscattered photons with anti-Compton spectrometer. IEEE Trans. Nucl. Sci. **38**, 386 (1991). https://doi.org/10.1109/23.289330
8. H. Utsunomiya, S. Goriely, T. Kondo et al., Photoneutron cross sections for Mo isotopes: A step toward a unified understanding of (γ, n) and (n, γ) reactions. Phys. Rev. C **88**, 015805 (2013). https://doi.org/10.1103/PhysRevC.88.015805
9. C. Angell, S. Hammond, H. Karwowski et al., Evidence for radiative coupling of the pygmy dipole resonance to excited states. Phys. Rev. C **86**, 051302 (2012). https://doi.org/10.1103/PhysRevC.86.051302
10. T. Kondo, H. Utsunomiya, S. Goriely et al., Total and partial photoneutron cross sections for Pb isotopes. Phys. Rev. C **86**, 014316 (2012). https://doi.org/10.1103/PhysRevC.86.014316
11. I. Gheorghe, H. Utsunomiya, S. Katayama et al., Photoneutron cross-section measurements in the $^{209}Bi(\gamma, xn)$ reaction with a new method of direct neutron-multiplicity sorting. Phys. Rev. C **96**, 044604 (2017). https://doi.org/10.1103/PhysRevC.96.044604
12. M. Krzysiek, H. Utsunomiya, I. Gheorghe et al., Photoneutron cross-section measurements for ^{165}Ho by the direct neutron-multiplicity sorting at NewSUBARU. Acta Phys. Pol. B **50**, 487 (2019). https://doi.org/10.5506/aphyspolb.50.487

13. I. Gheorghe, H. Utsunomiya, K. Stopani et al., Updated neutron-multiplicity sorting method for producing photoneutron average energies and resolving multiple firing events. Nucl. Instrum. Methods A **1019**, 165867 (2021). https://doi.org/10.1016/j.nima.2021.165867
14. A. Banu, J. Silano, H. Karwowski et al., Cross-section measurements of the ^{94}Mo(γ, n) and ^{90}Zr(γ, n) reactions using real photons at the HIγS facility. EPJ Web Conf. **178**, 03007 (2018). https://doi.org/10.1051/epjconf/201817803007
15. A. Banu, E. Meekins, J. Silano et al., Photoneutron reaction cross section measurements on ^{94}Mo and ^{90}Zr relevant to the *p*-process nucleosynthesis. Phys. Rev. C **99**, 025802 (2019). https://doi.org/10.1103/PhysRevC.99.025802
16. G. Matthieu, The abundance of ^{26}Al-rich planetary systems in the Galaxy. Astron. Astrophys. **582**, A26 (2015). https://doi.org/10.1051/0004-6361/201526174
17. H.Y. Lan, D. Wu, J.X. Liu et al., Photonuclear production of nuclear isomers using bremsstrahlung induced by laser-wakefield electrons. Nucl. Sci. Tech. **34**, 74 (2023). https://doi.org/10.1007/s41365-023-01219-x
18. W. Luo, Production of medical radioisotope ^{64}Cu by photoneutron reaction using ELI-NP γ-ray beam. Nucl. Sci. Tech. **27**, 96 (2016). https://doi.org/10.1007/s41365-016-0094-6
19. B. Ishkhanov, V. Varlamov, Photonuclear reactions: Modern status of the data. Phys. At. Nucl. **67**, 1664 (2004). https://doi.org/10.1134/1.1806905
20. H.W. Wang, G.T. Fan, L.X. Liu et al., Commissioning of laser electron gamma beamline SLEGS at SSRF. Nucl. Sci. Tech. **33**, 87 (2022). https://doi.org/10.1007/s41365-022-01076-0
21. Z.R. Hao, G.T. Fan, H.W. Wang et al., Collimator system of SLEGS beamline at Shanghai Light Source. Nucl. Instrum. Methods A **1013**, 165638 (2021). https://doi.org/10.1016/j.nima.2021.165638
22. H.H. Xu, G.T. Fan, H.W. Wang et al., Interaction chamber for laser Compton slant-scattering in SLEGS beamline at Shanghai Light Source. Nucl. Instrum. Methods A **1033**, 166742 (2022). https://doi.org/10.1016/j.nima.2022.166742
23. L.X. Liu, H.W. Wang, G.T. Fan et al., The SLEGS beamline of SSRF. Nucl. Sci. Tech. **35**, 111 (2024). https://doi.org/10.1007/s41365-024-01469-3
24. Z.R. Hao, H.H. Xu, G.T. Fan et al., Gamma spot monitor at SLEGS beamline. Nucl. Instrum. Methods A **1068**, 169748 (2024). https://doi.org/10.1016/j.nima.2024.169748
25. Z.C. Li, Y. Yang, Z.W. Cao et al., Effective extraction of photoneutron cross-section distribution using gamma activation and reaction yield ratio method. Nucl. Sci. Tech. **34**, 170 (2023). https://doi.org/10.1007/s41365-023-01330-z
26. X. Pang, B.H. Sun, L.H. Zhu et al., Progress of photonuclear cross sections for medical radioisotope production at the SLEGS energy domain. Nucl. Sci. Tech. **34**, 187 (2023). https://doi.org/10.1007/s41365-023-01339-4
27. S. Amano, K. Horikawa, K. Ishihara et al., Several-MeV γ rays generation at NewSUBARU by laser Compton backscattering. Nucl. Instrum. Methods A **602**, 337 (2009). https://doi.org/10.1016/j.nima.2009.01.010
28. L.X. Liu, H. Utsunomiya, G.T. Fan et al., Energy profile of laser Compton slant-scattering γ-ray beams determined by direct unfolding of total-energy responses of a BGO detector. Nucl. Instrum. Methods A **1063**, 169314 (2024). https://doi.org/10.1016/j.nima.2024.169314
29. W. Luo, H.Y. Lan, Y. Xu et al., Implementation of the n-body Monte-Carlo event generator into the Geant4 toolkit for photonuclear studies. Nucl. Instrum. Methods A **849**, 49 (2017). https://doi.org/10.1016/j.nima.2017.01.010
30. S. Agostinelli, J. Allison, K.A. Amako et al., Geant4-a simulation toolkit. Nucl. Instrum. Methods A **506**, 250 (2003). https://doi.org/10.1016/S0168-9002(03)01368-8
31. W. Luo, D.L. Balabanski, D. Filipescu, A data-based photonuclear simulation algorithm for determining specific activity of medical radioisotopes. Nucl. Sci. Tech. **27**, 113 (2016). https://doi.org/10.1007/s41365-016-0111-9
32. Z.R. Hao, L.X. Liu, Y. Zhang et al., Photoneutron dataset generation and analysis at SLEGS. ChinaXiv:202412.00386. https://doi.org/10.12074/202412.00386
33. O. Itoh, H. Utsunomiya, H. Akimune et al., Photoneutron cross sections for Au revisited: measurements with laser Compton scattering γ-rays and data reduction by a least-squares method. J. Nucl. Sci. Technol. **48**, 834 (2011). https://doi.org/10.1080/18811248.2011.9711766
34. Z.R. Hao, G.T. Fan, L.X. Liu, et al., Design and simulation of 4π flat-efficiency ^{3}He neutron detector array, Nucl. Tech. **43**, 9 (2020) (**in Chinese**). https://doi.org/10.11889/j.0253-3219.2020.hjs.43.110501
35. B. Berman, J. Caldwell, R. Harvey et al., Photoneutron cross sections for ^{90}Zr, ^{91}Zr, ^{92}Zr, ^{94}Zr, and ^{89}Y. Phys. Rev. **162**, 1098 (1967). https://doi.org/10.1103/PhysRev.162.1098
36. T. Renstrøm, H. Utsunomiya, H.T. Nyhus et al., Verification of detailed balance for γ absorption and emission in Dy isotopes. Phys. Rev. C **98**, 054310 (2018). https://doi.org/10.1103/PhysRevC.98.054310
37. G.C. Yang, L.M. Hua, F. Lu et al., Response functions of a 4π summing gamma detector in β-Olso method. Nucl. Sci. Tech. **33**, 68 (2022). https://doi.org/10.1007/s41365-022-01058-2
38. TENDL-2021. https://tendl.web.psi.ch/tendl_2021/gamma_html/gamma.html (2021)
39. J. Baglin, M. Thompson, B. Spicer, Photodisintegration of ^{27}Al:(I) photoneutron cross section. Nucl. Phys. **22**, 207 (1961). https://doi.org/10.1016/0029-5582(61)90453-9
40. N. Mutsuro, K. Kageyama, M. Mishina et al., Structure of giant resonance in ^{27}Al (γ, n) reaction. J. Phys. Soc. Jpn. **17**, 1672 (1962). https://doi.org/10.1143/JPSJ.17.1672
41. S. Fultz, J. Caldwell, B. Berman et al., Photoneutron cross sections for ^{12}C and ^{27}Al. Phys. Rev. **143**, 790 (1966). https://doi.org/10.1103/PhysRev.143.790
42. A. Veyssiere, H. Beil, R. Bergere et al., A study of the photoneutron contribution to the giant dipole resonance of sd shell nuclei. Nucl. Phys. A **227**, 513 (1974). https://doi.org/10.1016/0375-9474(74)90774-X
43. Z.Z. Li, Y.F. Niu, G. Colò, Toward a unified description of isoscalar giant monopole resonances in a self-consistent quasiparticle-vibration coupling approach. Phys. Rev. Lett. **131**, 082501 (2023). https://doi.org/10.1103/PhysRevLett.131.082501
44. V. Varlamov, B. Ishkhanov, V. Orlin, Reliability of (γ, 1n),(γ, 2n), and (γ, 3n) cross-section data on ^{159}Tb. Phys. Rev. C **95**, 054607 (2017). https://doi.org/10.1103/PhysRevC.95.054607